Soft Matter

ARTICLE

Use of extension-deformation-based crystallisation of silk fibres to differentiate their functions in nature

Received 00th January 20xx,
Accepted 00th January 20xx

DOI: 10.1039/x0xx00000x

www.rsc.org/

Keiji Numata,[*a] Hiroyasu Masunaga,[b] Takaaki Hikima,[c] Sono Sasaki,[cd] Kazuhide Sekiyama,[e] Masaki Takata[bc]

β-Sheet crystals play an important role in determining the stiffness, strength, and optical properties of silk and exhibit silk type-specific functions. It is important to elucidate the structural changes that occur during the stretching of silk fibres to understand the functions of different types of fibres. Here, we elucidate the initial crystallisation behaviour of silk molecules during the stretching of three types of silk fibres, using synchrotron radiation X-ray analysis. When spider dragline silk was stretched, it underwent crystallisation, and the alignment of the β-sheet crystals became disordered initially but recovered later. On the other hand, silkworm cocoon silk did not exhibit further crystallisation, while capture spiral silk was predominantly amorphous. Structural analyses showed that the crystallisation of the silks following extension deformation has a critical effect on their mechanical and optical properties. These findings should aid the production of artificial silk fibres and facilitate the development of silk-inspired functional materials.

Introduction

Silk and silk-like proteins are produced by many organisms in nature, including by spiders, silkworms, bees, ants, scorpions, and mussels. The silks of these organisms exhibit different mechanical and biological properties owing to the differences in their hierarchical structures, which are originated from amino acid sequences and spinning conditions.[1,2] A comparison of the stress-strain curves of the various silks indicated that spider dragline silk (Fig. 1a) is stronger and less pliable than spider capture silk (Fig. 1b), which is elastic and rubber like.[3] These diverse mechanical properties of silks are strongly related to their respective functions in nature. For example, dragline silk needs to be tough enough to be able to support a dangling spider, while capture silk should able to stretch and absorb energy so that it can be used to make strong and optically characteristic spider webs.[3,4] Silkworm cocoon silk (Fig. 1c), which is the tough outer component of the cocoon, is capable of protecting silkworms from external physical impact and predators.[2,5]

The hierarchical structures of silks vary with the silk type and determine their outstanding physical properties.[1,6] Among the most critical components of the hierarchical structures of silk are β-sheet crystals, since they play a significant role in determining silk stiffness, strength, and mechanical toughness.[7-9] Aligned β-sheet crystals provide stiffness and form cross-links between the β-sheet domains embedded in a semi-amorphous matrix that consists of less orderly structures, namely, random coils, helices, and β-turns.[8,9] Analyses of the amino acid sequences and structures of the cocoon silk of the *Bombyx mori* silkworm and the dragline silk of the *Nephila clavata* spider have shown that the β-sheet structure is predominant in both fibre types.[8,10,11] The strongest spider dragline silk is reported to be ~45–65% β-sheet domains,[12] whereas capture silk contains 54.4 mol% glycine and 16.6 mol% proline, resulting in predominantly β-spiral structures that resemble molecular springs.[13,14] Capture silk does not contain poly(alanine) sequences; however, the beta-sheet structure was found to contribute to the strength of capture silk fibres on the basis of Raman spectromicroscopy measurement.[15] Thus, the crystallisation of silk molecules is a critical molecular transition that dictates the physical, biological, and functional properties of silk.

In addition to nuclear magnetic resonance,[9,16-19] transmission electron microscopy,[20] and Raman and infrared spectroscopies,[8,21-23] synchrotron radiation X-ray scattering[11,24-34] has been used to characterise the structure of silk molecules and, in particular, those of β-sheet structures under extrusion conditions. The molecular structures of silkworm cocoon silk and spider dragline silk during deformation were investigated by several groups.[35-40] Lefèvre et al. investigated a monofilament of silkworm cocoon silk during stretching deofrmatin by Raman spectroscopy and suggested decreases in

[a] Enzyme Research Team, Biomass Engineering Program Cooperative Division, RIKEN Center for Sustainable Resource Science, 2-1 Hirosawa, Wako-shi, Saitama 351-0198, Japan.
[b] Japan Synchrotron Radiation Research Institute, 1-1-1, Kouto, Sayo-cho, Sayo-gun, Hyogo 679-5198, Japan.
[c] RIKEN SPring-8 Center, RIKEN 1-1-1 Kouto, Sayo-cho, Sayo-gun, Hyogo 679-5198, Japan.
[d] Graduate School of Science and Technology, Kyoto Institute of Technology, 1, Hashigami-cho, Matsugasaki Sakyo-ku, Kyoto 606-8585, Japan.
[e] Spiber Inc. 246-2 Mizukami, Kakuganji, Tsuruoka, Yamagata 997-0052, Japan.
† Electronic Supplementary Information (ESI) available: Fig. S1 and S2. See DOI: 10.1039/x0xx00000x

protein-chain alignment including β-sheet crystals due to the reorganization of the amorphous phase.[35] X-ray and neutron scattering measurements of bundle of silk fibres provided that amorphous phase of silk plays an important role to exhibit the toughness during stretching deformation.[36,37] Using single filaments of silk with Raman spectroscopy, Sirichaisit et al. successfully detected the structural change in spider dragline silk during approximately 25% stretching deformation.[38, 39]

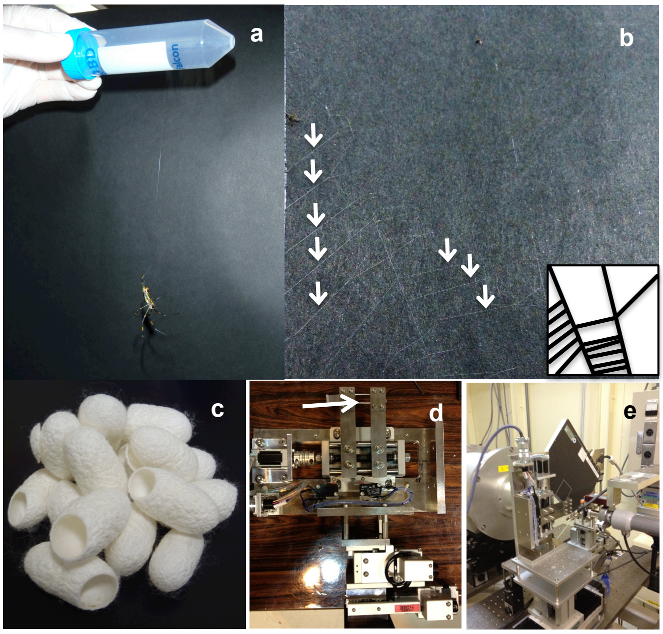

Fig. 1 Silk fibres and stretching equipment. (a) *Nephila clavata* dragline silk. (b) *N. clavata* web. The inset shows a schematic illustration of the web. The white arrows indicate capture silk fibres. (c) *Bombyx mori* silkworm cocoon silk. (d) The stretching machine used for the wide-angle X-ray scattering (WAXS) measurements of bundles of the silk fibres. The white arrow indicates the sample holder. (e) Synchrotron WAXS instrument with the stretching machine.

However, there are no reports on the relationship between stretching deformation, the formation of β-sheets, and silk function, especially during the initial stage of the stretching deformation. It is clear that the toughness of spider dragline silk is higher at high extension rates, a property that is unique among spider draglines.[41-43] This increase in toughness could be related to the initial crystallisation behaviour of dragline silk. We hypothesise that the crystallisation behaviour of silk molecules determines their mechanical properties as well as the function of the silk fibres in nature. This would be analogous to crystal formation in synthetic polymers such as the commodity plastics use in industry. On the basis of the results of the present study on the crystallisation behaviour of silk molecules during the stretching of silk fibres, we suggest that there exist different relationships between the crystallisation behaviour of the three investigated silk types and their natural function. First, crystallisation was induced owing to stretching deformation. The alignment of the β-sheet crystals was initially disordered but recovered later; this behaviour was observed only in spider dragline silk. Second, the fact that capture silk does not crystallise when subjected to stretching deformation is likely related to the fact that optical property of these silk fibres is not disturbed by any stretching deformation for capturing prey. Finally, the complete crystallisation of silkworm silk is likely an adaptive mechanism that protects the silkworm from external threats, such as bacterial infections,[44] physical attacks,[3, 45] and thermal and humidity changes.[46-48]

Experimental section

Sample preparation

The spider dragline silk was collected from *N. clavata* females. The spiders were released, and the dragline was collected at approximately 15 mm/s. According to previous reports,[30, 31] this drawing rate is within the range at which a linear increase in the orientational order is noticed with increases in the reeling speed indicating that the silk molecules are aligned along the fibre axis. Thus, the structure of the fibres was similar to that of natural spider dragline silk. The capture spiral silk was also collected from a web made by *N. clavata* females (Fig. 1b). Both types of spider silks were collected a day prior to the experiments and were kept in lightproof boxes with a wet sponge to prevent UV damage to the samples and to prevent them from drying. The silkworm cocoon silk was obtained from *B. mori* cocoons (Fig. 1c). The silk fibres were bundled manually using a bobbin (approximately 20 mm of diameter) before use. Ten spider silk fibres and three silkworm cocoon silk fibres were bundled as a bundle sample.

Synchrotron WAXS and SAXS measurements

The synchrotron wide angle X-ray scattering (WAXS) and small angle X-ray scattering (SAXS) measurements were performed at the BL45XU beamline of SPring-8, Harima, Japan using an X-ray energy of 12.4 keV (wavelength 0.1 nm); a beam with a diameter of 45 μm was employed. A beam with this diameter was sufficient to characterise the silk fibre bundles. A sample-stretching apparatus was placed on an X-Z positioning stage in the experimental hutch (Figs. 1d and 1e) and controlled from outside the experimental hutch. The silk fibres were attached to the stretching apparatus. The initial length of the silk fibres between the fixtures was 3.0 mm. The fibres were extended after being attached to the stretching apparatus. The extension rate was 1 mm/min. All the WAXS patterns were recorded with a flat-panel detector (FPD, C9728DK-10, Hamamatsu Photonics, Japan). The sample-to-detector distances during the WAXS and SAXS measurements were 50.2 and 2036 mm, respectively. The exposure time for each scattering pattern was 10 s. The radiation damage to the samples was evaluated for exposure times of up to 60 s; through a control experiment, it was determined than no structural changes occurred in the samples after exposure to radiation. The measurements were performed at 25ºC and a relative humidity of approximately 40%. According to previous reports,[49-51] a relative humidity of 40% has no effect on the mechanical properties of the silks, and is suitable for assessing the structural changes induced during the stretching process. The obtained 2D scattering patterns were converted into 1D profiles using the software Fit2D.[52]

Corrections were made for background scattering and the geometry of the detector. The azimuthal intensity profiles were obtained in the q-region from 15 nm^{-1} to 18 nm^{-1}. The intensities and full width at half maximum (FWHM) values of all the peaks were estimated through fitting using Gaussian profiles (Fig. S1†). For the Gaussian fitting, the number of band was one for each, and the position of the band was around -40 degree as the initial setting. The adjustment of fitting was performed by KaleidaGraph, according to a previous study.[26]

Results

Structural changes induced by extension

The changes in the crystal lattices of the dragline silk of *N. clavata*, spider capture spiral silk, and the cocoon silk of the *B. mori* silkworm during extension were characterised by synchrotron WAXS, which was performed at 25ºC and a relative humidity of 40%. Fibres with a length of 3.0 mm were stretched at 200-μm (dragline and cocoon silks) or 500-μm increments (capture silk) using laboratory-made stretching equipment until breakage (Figs. 1d and e). The silks demonstrated unusual extensibility, which indicated that the bundle samples were partially broken during the stretching. The reason to use the bundle samples in this experiment was to obtain scattering intensities enough for crystallinity and crystal orientation of silk fibres. The radiation damage to the single spider dragline silk fibres was investigated using exposure times of 2–60 s (Fig. S2†); no significant damage to the silk was detected, indicating that the short-multistep measurements in this study did not have significant damage. By the circular averaging of the two-dimensional (2D) WAXS patterns (Fig. 2), one-dimensional (1D) WAXS profile data for the fibres before and during stretching were obtained (Fig. 3). Based on the difference between before and after the stretching deformation (Fig. 2d), the crystallisation of dragline silk was obvious, whereas the decrease in the intensity of silkworm silk was due to a decrease in sample amount by stretching fibres (Fig. 2h). The decrease in the intensity was reasonable when the crystal was not formed. This is because the amount of fibres on the X-ray beam was also decreased by the stretching deformation. The WAXS profile of dragline silk was similar to that of β-poly(L-alanine), that is, both exhibit (020), (210), and (040) reflections (Fig. 3a).[32] When the dragline silk fibre was stretched, there was no change in its crystalline structure. Further, bundles of dragline fibres broke after a stretching deformation of 133%. The samples were not single fibres but bundle of fibres, leading to such a high extensibility. The d-spacings of the (210) and (020) planes were 0.40 nm and 0.51 nm before and during deformation, respectively, suggesting that the β-sheet crystal composition of the dragline silk fibres did not change. The WAXS pattern of the silkworm silk showed (020), (210), (030), and (040) reflections; these are indicative of a silk II structure composed of antiparallel β-sheets.[27, 29] The d-spacing of the (020) plane was 0.39 nm and remained constant. Further, the (020) reflection became broader during the stretching process (Fig. 2e-h and Fig. 3b). This indicates that a fraction of the β-sheet crystals in the silkworm silk deform into a more tightly packed crystalline state with lower d-spacings.

An amorphous halo was present before and during the stretching of the capture silk, and no crystalline components were noticed, indicating that capture silk is a completely amorphous biopolymer under the experimental conditions employed (Fig. 4). The sharp peaks detected in the profiles of the capture silk may be due to crystalline aggregation and the presence of impurities attached to the web.

Crystallinity

From the 1D intensity profiles shown in Fig. 3, we calculated the crystallinities of the spider dragline and silkworm cocoon silks before and during deformation (Fig. 5). Each intensity profile was separated into crystalline and amorphous scattering components by curve fitting methods using Gaussian functions. The ratio of the total area of the separated crystalline scattering components to that of the crystalline and amorphous scattering components was used to determine the crystallinity. According to a previous report, the short-range-ordered components, such as β-sheet protocrystals,[53] β-spirals,[54] coiled structures,[55] and α-helical chains,[56] can be detected as a broad peak in the crystalline component in the WAXS profile.[29] However, in the present study, the change in the broad peak corresponding to the short-range-ordered structure during the stretching deformation was too small to be characterised. Although it has previously been reported that the separation of the peaks of the WAXS profiles of silk fibres is challenging,[26] there have been several reports on the crystal contents of silk fibres. The crystallinity of dragline silk was predicted to be 45% by modelling spider silk's mechanical properties with an amorphous matrix,[57] whereas the crystallinities determined by transmission electron microscopy and solid-state ^{2}H NMR were approximately 50 and 35 %, respectively.[53, 58] In the case of FTIR characterization, the beta- sheet contents of *B. mori*, *Antheraea pernyi* silkworm silk, and *Nephila edulis* spider silk (major ampullate filaments) were determined to be 28 ± 4, 23 ± 2, and 17 ± 4%, respectively.[21] The beta-sheet content of *A. pernyi* silkworm silk during its deformation was constant and

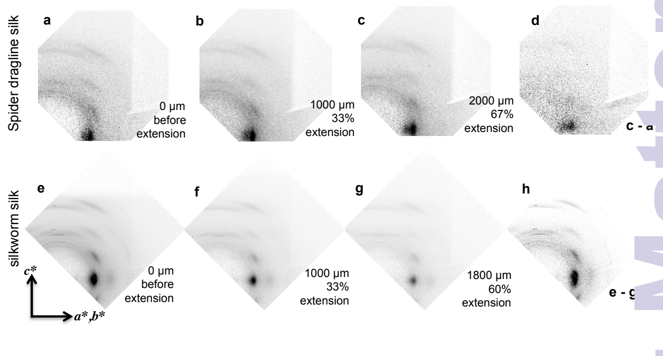

Fig. 2 2D WAXS patterns of spider dragline silk (a-d) and silkworm cocoon silk (e-h). (a and e) The patterns of the fibres before stretching deformation. (b, c, f, and g) The patterns during the extension of the fibres. (d) The pattern subtracted (a) from (c). (h) The pattern subtracted (g) from (e).

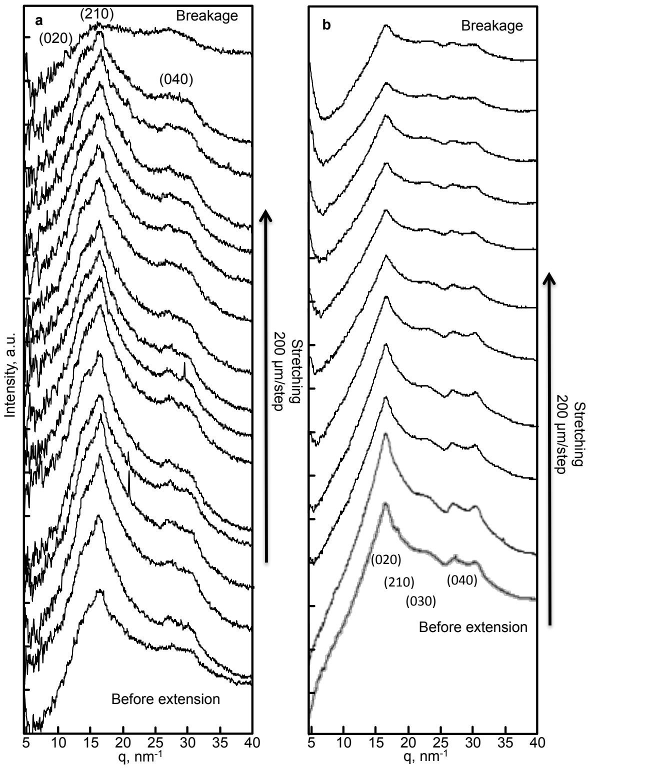

Fig. 3 One-dimensional WAXS profiles derived from the 2D WAXS patterns of (a) spider dragline silk and (b) silkworm cocoon silk before and during stretching deformation. The profiles on the bottom profiles are the profiles before the stretching deformation. Moving from the bottom to the top, the profiles represent the samples as they were stretched until breakage. The profiles were fitted using the Gaussian function as a broad peak owing to the presence of a halo and the Bragg reflections (a) (020)/(210)/(040) in the case of dragline silk and (b) (020)/(210)/(030)/(040) in the case of silkworm silk.

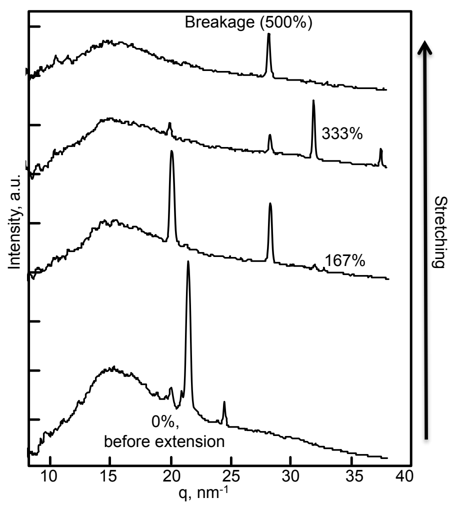

Fig. 4 One-dimensional WAXS profiles derived from the 2D WAXS patterns of spider capture silk before and during stretching deformation. The profiles on the bottom profiles are the profiles before the stretching deformation. Moving from the bottom to the top, the profiles represent the samples as they were stretched until breakage.

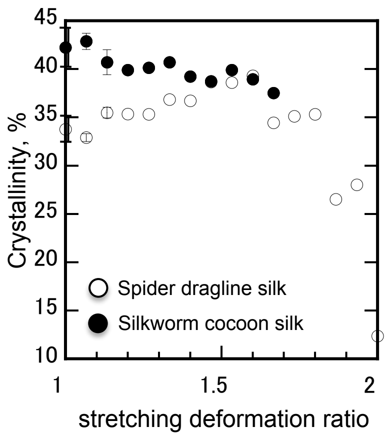

Fig. 5 Crystallinity of spider dragline (open circles) and silkworm silks (closed circles) before and during stretching deformation. The stretching deformation ratio of 1.0 corresponds to the original state before the stretching deformation and a stretching deformation ratio of 1.5 is equivalent to stretching by 50%. The error bars represent the standard deviations for the samples (n = 3).

around 38 %.[59] When beta-sheet crystals of *B. mori* silkworm cocoon silk were prepared by methanol treatment of the silk solution, the crystallinity was determined to be 53 ± 8%.[60] Here, we monitored the change in the crystallinity during the stretching process. Although this means the obtained values are relative rather than absolute ones, they are sufficient to gain an insight into the relative changes in the crystallinity. The crystallinity of a bundle of dragline silk fibres increased from approximately 32% to 40% upon stretching, after which the fibres broke at an elongation ratio of 1.6 (i.e., after an extension of 60%). On the other hand, the crystallinity of a bundle of the silkworm silk fibres decreased with the elongation ratio; this indicates that β-sheet formation was not induced to a significant degree by the stretching. The decrease in the crystallinity of the silkworm silk could be due to the decrease in the volume of the bundle of the silk fibres because of the stretching deformation.

Crystal orientation with respect to the fibre axis

To evaluate the orientation of the β-sheet crystals with respect to the fibre axis, the (210) reflections of the dragline and silkworm silks were characterised in terms of the full width at half maximum (FWHM) on the equatorial line as an orientation parameter (Fig. S1†). The FWHM values and peak intensities of the azimuthal intensity profiles of the (210) reflections of the spider dragline and silkworm cocoon silks are plotted as functions of the stretching deformation ratio in Fig. 6. The FWHM of the spider dragline silk increased after the initial stretching step, indicating that the initial stretching deformation misaligned the β-sheet crystals with respect to the fibre axis (Fig. 6a). After the initial stretching, the FWHM of the spider dragline silk decreased gradually, indicating that the β-sheet structure was reoriented during the stretching process. A decrease in the FWHM of the (210) peak of the silkworm silk with an increase in the stretching deformation ratio indicated that the β-sheet crystals were more highly oriented along the fibre axis following the stretching deformation (Fig. 6b).

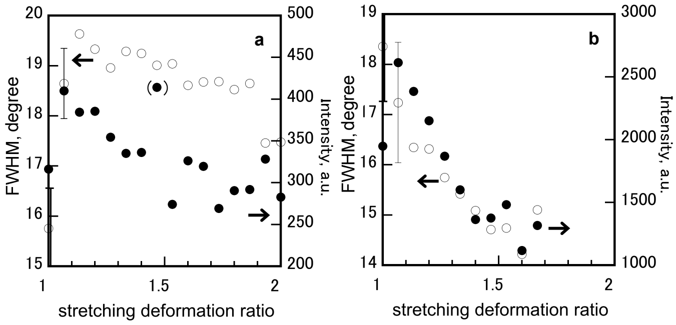

Fig. 6 Orientation of spider dragline (a) and silkworm silks (b) before and during stretching deformation. (a) FWHM values (open circles) and intensities (closed circles) determined from the spider dragline silk (210) reflection as a function of the stretching deformation ratio. The FWHM value represents the degree of orientation of β-sheet crystals along the fibre axis. (b) FWHM values (open circles) and intensities (closed circles) determined from the silkworm silk (210) reflection as a function of the stretching deformation ratio. The error bars represent the standard deviations for the samples (*n* = 3).

Microscale morphology

To study the larger-scale morphologies of the silks, synchrotron SAXS measurements were performed on the silks (Fig. 7). The SAXS pattern for an unstretched spider dragline silk fibre (Fig. 7a) exhibits streak scatterings along the equator and the fibre axis. The small streak along the fibre axis disappeared after the stretching of the fibre (Fig. 7b). The pre- and post-stretching SAXS patterns of the silkworm silk fibre exhibited two types of streak scatterings along the equator and the fibre axis (Figs. 7c and d). Further, the streak scattering of the silkworm silk was broader than that of the spider dragline silk.

The streak scattering along the equator axis remained sharp, indicating that the fibres were oriented as a bundle along one direction, even though 10 spider dragline silks and 3 silkworm silks were used as a bundle sample. Additionally, the sharpness of the streaks maintained before and after the stretching. These results related to SAXS indicate that fibre orientation of the samples were sufficient to be discussed including the orientations of the crystals along the fibre axis.

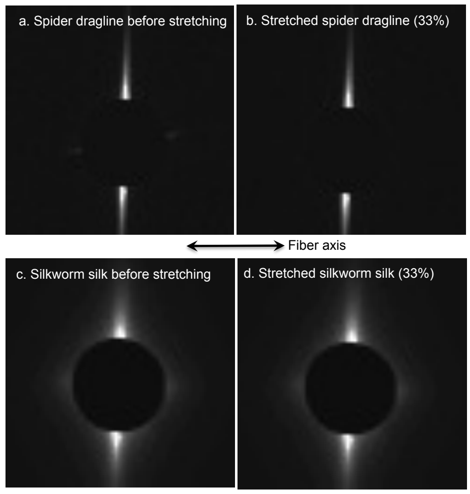

Fig. 7 SAXS patterns of spider dragline silk (a,b) and silkworm silk fibres (c,d) before (a,c) and during stretching deformation (33%, b and d).

Discussion

Dragline silk, capture silk, and silkworm silk undergo different structural changes in response to stretching deformation. The samples were not single fibres but bundle of fibres, leading to a higher extensibility in comparison to the single fibre.[3] The bundled fibres after their partial digestion were fully stretched; however, the following crystallization was not easy to be discussed. This is because the stretching deformation rate was not precisely quantified. Therefore, we focused the initial deformation part and discussed the change of crystallinity of silk fibres and alignments of beta-sheet crystals. The deformation induced crystallisation in the dragline silk; however, its crystal structure did not change significantly (Fig. 2a). On the other hand, the crystallinity of the dragline silk increased slightly, and the orientation of the β-sheet crystals became dramatically disordered after the initial stretching deformation (Figs. 5 and 6a). The crystallisation of dragline silk might include the short-range-ordered components. This indicates that the initial deformation of the dragline silk did not align the β-sheet crystals along the fibre axis, but induced the formation of additional β-sheets instead (Fig. 8a). It has been reported that tensile deformation increases the orientation of the crystals along the fibre axis in *N. clavata* spider silk when the silk fibres are extended by 10%.[26] In this study, stretching resulting in deformation greater than 60% (deformation ratio of 1.6) induced the formation of ~10% additional crystalline components, leading to the realignment of the spider dragline silk fibres (Fig. 5). Taking into the account the natural function

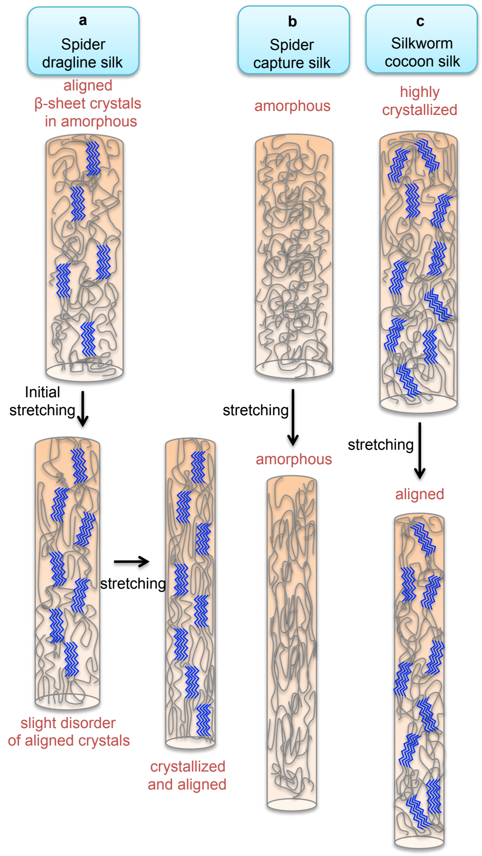

Fig. 8 Schematic illustration of (a) spider dragline silk, (b) spider capture silk, and (c) silkworm cocoon silk before and during stretching deformation.

of spider dragline silk, we infer that the β-sheet formation induced by the initial stretching deformation is related to the stretching-rate sensitivity of the silk dragline fibres.[41] The size and amount of crystalline silk were reported to decrease and increase with an increase in drawing rate,[61, 62] indicating that non-crystalline silk which can be crystallised is present in silk fibres. The rupture energy of dragline silk increases when the silk fibres are tested at higher strain rates.[41-43] This suggests that a faster extension deformation would induce the formation of a greater number of β-sheets and cause the subsequent alignment of the β-sheet crystals in the dragline, resulting in higher mechanical strength. Thus, the initially detected structural disorder and alignment could be related to the effects of the extension rate on the mechanical properties, because the initial alignment of the β-sheet crystals depends on the initial stretching rate when the silk fibres contain a sufficient number of amorphous and short-range-ordered structures. Furthermore, spider dragline silk crystallises during stretching; this probably prevents it from undergoing excessive elongation and may act as a ‘braking' mechanism when the silk is used in nature.

Riekel et al. did not mention any initial disordering effects after forced silking experiments.[30] However, the stretching of the spider dragline silk fibre is not exactly similar to the forced silking of spider silk. This is because forced silking is performed during the spinning process or just after the spinning. Therefore, it differs from the stretching of the dragline silk fibres, and, in particular, the stretching of the fibre surfaces after their crystallisation in air. Further, initial disordering effects were not observed in a molecular modelling study either.[57] This is because the alignment of the β-sheet crystals was simplified and considered parallel along the fibre axis. As a result, no initial disordering effects were observed using the molecular models.

In addition to the alignment of the β-sheet crystals, a role of amorphous region is also significant to explain the structural change during stretching deformation. Lefèvre et al. reported that the alignment of the silk molecules decreases with stretching deformation, which might be due to the reorganization of the amorphous phase.[35] Seydel et al. also recognized the importance of the amorphous phase of silk fibres during stretching deformation, namely, most of the deformation upon extension of the fibres is due to the amorphous regions of the silk, based on X-ray diffraction and neutron spectroscopy measurements.[36,37] Based on our current results and previous reports on transition of molecular structure of silkworm and spider dragline silks,[38,39] the change of crystallinity indicates that molecular deformation and structural transition of silk molecules during stretching deformation. Considering the previous reports mentioned above, the initial disorder we found here can be explained as follows: the amorphous region of silk is disordered by the initial deformation, resulting in the disorder of the β-sheet crystal alignment. Until now, the previous literatures indicated the initial disorder of amorphous region, however, this report directly shows the initial disorder of silk’s β-sheet crystals.

Viscid silk and glues are noncrystalline and can only be crystallised partially at low temperatures, according to the unpublished data from a study by Craig and Riekel.[63] Here, we present the first structural analysis of spider capture silk during stretching deformation. We found that its structure is predominantly amorphous and is not converted to a crystalline state even when the silk is stretched by 500% (Fig. 8b). The amino acid sequence and composition of the capture silk of *N. clavata* differs from those of *N. clavata* dragline silk and *B. mori* silk. The amino acid sequences for the β-sheet formation found in *N. clavata* dragline silk and *B. mori* silk are AAAAA and GAGAGS, respectively; however, these are not found in *N. clavata* capture silk, which mostly contains glycine- and proline-rich β-spiral structures.[13, 14] The capture spiral silk does not exhibit any crystalline components and nor does it undergo crystallisation before and during the stretching deformation. This allows it to retain its elastic and optical properties during deformation. Spider webs made of capture silk are known to display multiple colours during the reflection, refraction, and transmission of sunlight.[64,65] The results of the structural analysis of capture silk demonstrate that this silk is perfectly amorphous during stretching. It is for this reason that crystallisation does not have an effect on the optical properties of spider webs of this silk. These attributes of capture silk, which is one of the main components of spider webs, ensure that it is better suited that other types of silks for catching prey.

Crystallisation was not induced in silkworm silk after stretching deformation; however, the orientation of the crystals and their alignment along the fibre axis became more ordered (Figs. 5 and 6b). This is similar to the effects of stretching on conventional crystalline polymers (Fig. 8c). This result indicates that the β-sheet crystals of silkworm silk are already present in the silkworm cocoons. The β-sheet crystals of silkworm silk must be formed by mainly the silkworm's spinning but also dehydration of spun silk fibres in air. The silk of silkworm cocoons must contain a sufficient number of crystalline regions in order to be able to protect the chrysalis from external physical impact and predators. It has thus not evolved to respond to stretching deformation. This conclusion is supported by the mechanical properties exhibited by the two types of silk fibres investigated, namely, the fact that *B. mori* silkworm silk breaks after elongation by ~15% and is less elastic,[66] in contrast to *N. edulis* spider dragline silk, whose average breaking elongation is approximately 40%.[67] Moreover, spinning speed was reported to exert a significant effect on the mechanical properties of silkworm silk.[2] Thus, we reconfirm that the silkworm cocoon silk has a high crystallinity and low elasticity; these properties are consistent with its role as a tough outer component of the chrysalis.

The effects of stretching deformation on the larger-scale morphologies of the different silks (Fig. 7) were different, as evidenced by their SAXS patterns. In the case of the spider dragline silk, the streak scattering along the equator could be considered to be due to voids in the fibres or at the interfaces of the fibres, in keeping with a previous report.[68] In addition, the small streak scattering might be due to voids or disordered structures along the fibre axis. These structural disorders in the spider dragline silk disappeared during stretching. On the other hand, the streak scattering of the silkworm silk, which was broader in comparison to that of the spider dragline silk, implied that a greater number of voids and holes exist in the silkworm silk fibres than do in the spider dragline silk fibres and that these structural disorders do not disappear after the stretching deformation. According to a previous report on the fracture surfaces of silkworm and spider dragline silks, some disordered structures among the silk microfibrils were observed.[69] Although we don't have a direct evidence to show that the streak scattering is originated from the disordered structures, it is one of the reasonable explanations. These structural disorders in the silkworm silk could prevent crystallisation and disturb the alignment of the silk molecules during the stretching deformation.

Conclusions

We have confirmed that the different crystallisation behaviours of different types of silk fibres following extension deformation are closely related to their functions in nature. Spider dragline silk undergoes significant structural changes during stretching deformation, particularly during the initial phase, which resulted in it exhibiting the highest strength among the silk fibres tested. The effects of the reeling and stretching speeds on the structure and mechanical properties of spider dragline silk remain to be elucidated;[58] however, they could be related to the initial disorder and alignment of the dragline silk fibres. The mechanism underlying the marked increase noticed in the toughness of spider dragline silk at high extension rates will be investigated in a future study. On the other hand, spider capture silk was confirmed to be perfectly amorphous before and during the deformation; this is consistent with the requirement that spider webs must maintain their optical properties and elasticity when under physical attack as well as following environmental deformation by the elements. Our findings provide critical insight into how the structure and function of silk fibres can be modulated; this should facilitate the design and construction of bioinspired materials that are tough but retain their elastic and optical properties.

Acknowledgements

This work was supported by Grants-in-Aid for Young Scientists (B) and Impulsing Paradigm Change through Disruptive Technologies Program (ImPACT) (K.N.).

Notes and references

1. Y. Liu, Z. Z. Shao and F. Vollrath, *Nat. Mater.*, 2005, **4**, 901-905.
2. Z. Shao and F. Vollrath, *Nature*, 2002, **418**, 741.
3. J. Gosline, M. Lillie, E. Carrington, P. Guerette, C. Ortlepp and K. Savage, *Phil. Trans. Royal Soc. B,* 2002, **357**, 121-132.
4. S. W. Cranford, A. Tarakanova, N. M. Pugno and M. J. Buehler, *Nature*, 2012, **482**, 72-76.
5. F. Chen, T. Hesselberg, D. Porter and F. Vollrath, *J. Exp. Biol.*, 2013, **216**, 2648-2657.
6. F. J. Chen, D. Porter and F. Vollrath, *Acta Biomater.*, 2012, **8**, 2620-2627.
7. S. Keten, Z. Xu, B. Ihle and M. J. Buehler, *Nat. Mater.*, 2010, **9**, 359-367.
8. T. Lefevre, M. E. Rousseau and M. Pezolet, *Biophys. J.*, 2007, **92**, 2885-2895.
9. J. D. van Beek, S. Hess, F. Vollrath and B. H. Meier, *Proc. Natl. Acad. Sci. USA*, 2002, **99**, 10266-10271.
10. O. Liivak, A. Blye, N. Shah and L. W. Jelinski, *Macromolecules*, 1998, **31**, 2947-2951.
11. C. Riekel, C. Branden, C. Craig, C. Ferrero, F. Heidelbach and M. Muller, *Int. J. Biol. Macromol.*, 1999, **24**, 179-186.
12. F. Vollrath and D. Porter, *Polymer*, 2009, **50**, 5623-5632.
13. N. Becker, E. Oroudjev, S. Mutz, J. P. Cleveland, P. K. Hansma, C. Y. Hayashi, D. E. Makarov and H. G. Hansma, *Nat. Mater.*, 2003, **2**, 278-283.
14. C. Y. Hayashi and R. V. Lewis, *Science*, 2000, **287**, 1477-1479.
15. T. Lefevre and M. Pezolet, *Soft Matter*, 2012, **8**, 6350-6357.
16. T. Asakura, A. Kuzuhara, R. Tabeta and H. Saito, *Macromolecules*, 1985, **18**, 1841-1845.
17. T. Asakura, J. Yao, T. Yamane, K. Umemura and A. S. Ulrich, *J. Am. Chem. Soc.*, 2002, **124**, 8794-8795.

18. J. E. Jenkins, S. Sampath, E. Butler, J. Kim, R. W. Henning, G. P. Holland and J. L. Yarger, *Biomacromolecules*, 2013, **14**, 3472-3483.
19. H. Yoshimizu and T. Asakura, *J. Appl. Polym. Sci.*, 1990, **40**, 1745-1756.
20. J. E. Trancik, J. T. Czernuszka, F. I. Bell and C. Viney, *Polymer*, 2006, **47**, 5633-5642.
21. S. Ling, Z. Qi, D. P. Knight, Z. Shao and X. Chen, *Biomacromolecules*, 2011, **12**, 3344-3349.
22. M. E. Rousseau, T. Lefevre and M. Pezolet, *Biomacromolecules*, 2009, **10**, 2945-2953.
23. J. Sirichaisit, V. L. Brookes, R. J. Young and F. Vollrath, *Biomacromolecules*, 2003, **4**, 387-394.
24. C. J. Benmore, T. Izdebski and J. L. Yarger, *Phys. Rev. Let.*, 2012, **108**.
25. A. Bram, C. I. Branden, C. Craig, I. Snigireva and C. Riekel, *J. Appl. Crystallogr.*, 1997, **30**, 390-392.
26. D. T. Grubb and L. W. Jelinski, *Macromolecules*, 1997, **30**, 2860-2867.
27. R. E. Marsh, R. B. Corey and L. Pauling, *Biochim. Biophys. Acta*, 1955, **16**, 1-34.
28. A. Martel, M. Burghammer, R. J. Davies, E. Di Cola, C. Vendrely and C. Riekel, *J. Am. Chem. Soc.*, 2008, **130**, 17070-17074.
29. A. Martel, M. Burghammer, R. J. Davies and C. Riekel, *Biomacromolecules*, 2007, **8**, 3548-3556.
30. C. Riekel, B. Madsen, D. Knight and F. Vollrath, *Biomacromolecules*, 2000, **1**, 622-626.
31. C. Riekel, M. Muller and F. Vollrath, *Macromolecules*, 1999, **32**, 4464-4466.
32. C. Riekel and F. Vollrath, *Int. J. Biol. Macromol.*, 2001, **29**, 203-210.
33. Y. Takahashi, M. Gehoh and K. Yuzuriha, *Int. J. Biol. Macromol.*, 1999, **24**, 127-138.
34. Z. Yang, D. T. Grubb and L. W. Jelinski, *Macromolecules*, 1997, **30**, 8254-8261.
35. T. Lefevre, F. Paquet-Mercier, S. Lesage, M. E. Rousseau, S. Bedard and M. Pezolet, *Vib. Spectrosc.*, 2009, **51**, 136-141.
36. T. Seydel, K. Kolln, I. Krasnov, I. Diddens, N. Hauptmann, G. Helms, M. Ogurreck, S. G. Kang, M. M. Koza and M. Muller, *Macromolecules*, 2007, **40**, 1035-1042.
37. I. Krasnov, I. Diddens, N. Hauptmann, G. Helms, M. Ogurreck, T. Seydel, S. S. Funari and M. Muller, *Phys. Rev. Let.*, 2008, **100**.
38. J. Sirichaisit, R. J. Young and F. Vollrath, *Polymer*, 2000, **41**, 1223-1227.
39. J. Sirichaisit, V. L. Brookes, R. J. Young and F. Vollrath, *Biomacromolecules*, 2003, **4**, 387-394.
40. V. L. Brookes, R. J. Young and F. Vollrath, *J. Mater. Sci.*, 2008, **43**, 3728-3732.
41. J. M. Gosline, P. A. Guerette, C. S. Ortlepp and K. N. Savage, *J. Exp. Biol.*, 1999, **202**, 3295-3303.
42. M. Denny, *J. Exp. Biol.*, 1976, **65**, 483-506.
43. M. Hudspeth, X. Nie, W. N. Chen and R. Lewis, *Biomacromolecules*, 2012, **13**, 2240-2246.
44. J. Pandiarajan, B. P. Cathrin, T. Pratheep and M. Krishnan, *Rapid Commun. Mass Spec.*, 2011, **25**, 3203-3206.
45. C. S. Hieber, *Oecologia*, 1992, **91**, 530-535.
46. H. V. Danks, *Eur. J. Entomol.*, 2004, **101**, 433-437.
47. B. E. Lyon and R. V. Cartar, *Proc. Roy. Soc. B*, 1996, **263**, 1159-1163.
48. B. Blossman-Myer and W. W. Burggren, *Comp. Biochem. Phys. A*, 2010, **155**, 259-263.
49. C. J. Fu, D. Porter and Z. Z. Shao, *Macromolecules*, 2009, **42**, 7877-7880.
50. T. Vehoff, A. Glisovic, H. Schollmeyer, A. Zippelius and T. Salditt, *Biophys. J.*, 2007, **93**, 4425-4432.
51. T. Seydel, W. Knoll, I. Greving, C. Dicko, M. M. Koza, I. Krasnov and M. Muller, *Phys. Rev. E*, 2011, **83**.
52. A. P. Hammersley, *European Synchrotron Radiation Facility Internal Report*, 1997, **ESRF97HA02T**.
53. A. H. Simmons, C. A. Michal and L. W. Jelinski, *Science*, 1996, **271**, 84-87.
54. C. Y. Hayashi and R. V. Lewis, *J. Mol. Biol.*, 1998, **275**, 773-784.
55. Z. Y. Dong, R. V. Lewis and C. R. Middaugh, *Arch Biochem. Biophys.*, 1991, **284**, 53-57.
56. J. Kummerlen, J. D. van Beek, F. Vollrath and B. H. Meier, *Macromolecules*, 1996, **29**, 2920-2928.
57. Y. Termonia, *Macromolecules*, 1994, **27**, 7378-7381.
58. B. L. Thiel, K. B. Guess and C. Viney, *Biopolymers*, 1997, **41**, 703-719.
59. S. J. Ling, Z. M. Qi, D. P. Knight, Y. F. Huang, L. Huang, H. Zhou, Z. Z. Shao and X. Chen, *Biomacromolecules*, 2013, **14**, 1885-1892.
60. K. Numata, P. Cebe and D. L. Kaplan, *Biomaterials*, 2010, **31**, 2926-2933.
61. M. W. Denny, in *The machanical properties of biological materials*, ed. C. J. F. V. a. C. Vincent, J. D., Cambridge University Press, Cambridge, UK, 1980, pp. 247-272.
62. N. Du, X. Y. Liu, J. Narayanan, L. A. Li, M. L. M. Lim and D. Q. Li, *Biophys. J.*, 2006, **91**, 4528-4535.
63. C. L. Craig, *Spiderwebs and silk : tracing evolution from molecules to genes to phenotypes*, Oxford Univesity Press, Oxford England ; New York, 2003.
64. G. R. S. Deb M. Kane, Nishen Naidoo, Douglas J. Little, Marie E. Herberstein, *Proc. of SPIE*, 2011, **7975**.
65. C. L Craig, *Biotropica*, 1989, **21**, 257-264.
66. M. A. Wilding and J. W. S. Hearle, in *Polymeric Materials Encyclopedia*, ed. J. C. Salamone, CRC Press Inc., Boca Raton, Florida, 1996, vol. 11, pp. 8307-8322.
67. F. Vollrath, B. Madsen and Z. Z. Shao, *Proc. Roy. Soc. B*, 2001, **268**, 2339-2346.
68. T. Tanaka, K. Uesugi, A. Takeuchi, Y. Suzuki and T. Iwata, *Polymer*, 2007, **48**, 6145-6151.
69. P. Poza, J. Perez-Rigueiro, M. Elices and J. Llorca, *Eng. Fract. Mech.*, 2002, **69**, 1035-1048.

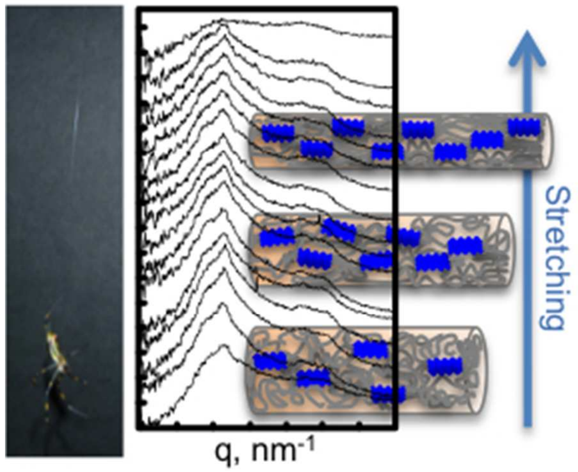

TOC
50x41mm (150 x 150 DPI)